2013

An Isolated Three-Port Bidirectional DC-DC Converter for Photovoltaic Systems with Energy Storage

Jianwu Zeng
University of Nebraska-Lincoln, jzeng@huskers.unl.edu

Wei Qiao
University of Nebraska–Lincoln, wqiao@engr.unl.edu

Liyan Qu
University of Nebraska-Lincoln, lqu2@unl.edu

2013-IACC-322
Industry Applications Society Annual Meeting, 2013 IEEE
Year: 2013
Pages: 1 - 8, DOI: 10.1109/IAS.2013.6682520

An Isolated Three-Port Bidirectional DC-DC Converter for Photovoltaic Systems with Energy Storage

Jianwu Zeng
Student Member, IEEE
Power & Energy Systems Laboratory
Department of Electrical Engineering
University of Nebraska-Lincoln
Lincoln, NE, 68588-0511, USA
jzeng@huskers.unl.edu

Wei Qiao
Senior Member, IEEE
Power & Energy Systems Laboratory
Department of Electrical Engineering
University of Nebraska-Lincoln
Lincoln, NE, 68588-0511, USA
wqiao@engr.unl.edu

Liyan Qu
Member, IEEE
Power & Energy Systems Laboratory
Department of Electrical Engineering
University of Nebraska-Lincoln
Lincoln, NE, 68588-0511, USA
lqu2@unl.edu

***Abstract*–This paper proposes a new isolated, three-port, bidirectional, DC-DC converter for simultaneous power management of multiple energy sources. The proposed converter has the advantage of using the least number of switches and soft switching of the main switch, which is realized by using a LCL-resonant circuit. The converter is capable of interfacing sources of different voltage-current characteristics with an isolated load. In this paper, one photovoltaic (PV) panel, one rechargeable battery, and an isolated load are interfaced by the proposed converter. Simulation and experimental results show that the proposed converter is capable of maximum power point tracking control for the PV panel when there is solar radiation and controlling the charge and discharge of the battery when there is surplus energy and power deficiency with respect to the load, respectively.**

***Index Terms*—Battery, bidirectional DC-DC converter, isolated converter, multiport converter, photovoltaic (PV), soft switching.**

I. INTRODUCTION

To integrate multiple DC energy sources of different types to a power grid, multiple independent DC-DC converters are commonly used to step up the time-variant, low-level source voltages to a constant high-level voltage that is required by a grid-tie inverter. Comparing to that solution, a multiport DC-DC converter is preferable owing to the advantages of using fewer components, lower cost, higher power density, and higher efficiency [1]-[2].

The multiport converter topologies can be classified into two categories: nonisolated and isolated topologies. Nonisolated multiport converters, which take the form of buck, boost, and buck-boost topologies, are used in the applications where a low voltage regulation ratio is required. In contrast, in those applications requiring a high voltage regulation ratio, isolated converters which contains a transformer is preferred.

The currently used isolated multiport topologies include the isolated full-bridge converter [3], which uses four controllable power switches for each source, the isolated half-bridge converter [4], which uses two switches for each source, and the isolated single-switch converter [5], which only uses one switch for each source. In some practical applications, energy storage, such as batteries, is commonly used to handle the intermittence of solar and wind energy sources. This requires that at least one port of the multiport converter is bidirectional. The aforementioned topologies are all unidirectional and cannot satisfy such applications [6].

Several bidirectional topologies, such as full-bridge [7]-[8] and half-bridge [9]-[10] topologies, have been proposed. These two topologies utilize many switches with complicated drive and control circuits. Recently, a three-port topology with only one middle branch added to the traditional half-bridge converter was proposed [11]. It uses less controllable power switches than the half-bridge topology and can achieve zero-voltage switching (ZVS) for all main switches. However, the voltage of the primary source should be maintained at a high value to charge the battery.

This paper proposes a new isolated, three-port, bidirectional, DC-DC converter topology, which has the same number of switches as the isolated, three-port, bidirectional, DC-DC converter proposed in [11]. However, compared with the converter in [11], the required voltage of the renewable energy source to charge the battery with the same nominal voltage is lower when using the proposed converter. Moreover, the proposed converter contains an inductor-capacitor-inductor (LCL)-resonant circuit to achieve ZVS and zero-current switching (ZCS) for the main switch. The proposed converter is applied for simultaneous power management of a PV system with battery storage in this paper. The PV panel and the battery are connected to the unidirectional port and the bidirectional port of the converter, respectively. A maximum power point tracking (MPPT) algorithm is designed for the PV panel to generate the maximum power when solar radiation is available. A charge and discharge controller is designed to control the battery to either absorb the surplus power generated by the PV panel or supply the deficient power required by the load. Simulation and experimental results are provided to validate the proposed converter.

This material is based upon work supported by the Federal Highway Administration under Agreement No. DTFH61-10-H-00003. Any opinions, findings, and conclusions or recommendations expressed in this publication are those of the authors and do not necessarily reflect the view of the Federal Highway Administration.

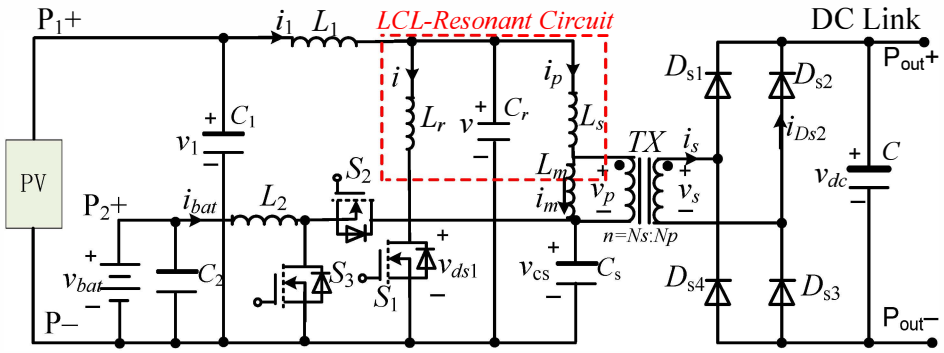

Fig. 1. Proposed isolated three-port bidirectional DC-DC converter for a PV and battery system.

II. Topology and Operating Principle of the Proposed Converter

A. Topology of the Proposed Converter

The circuit diagram of the proposed converter is shown in Fig. 1, which consists of a low-voltage-side (LVS) circuit and a high-voltage-side (HVS) circuit connected by a high-frequency transformer. The LVS consists of two ports, an energy storage capacitor C_S, the primary winding of the transformer, and a LCL-resonant circuit consisting of two inductors L_r and L_s and a capacitor C_r, where L_s is the leakage inductance of the transformer.

The HVS consists of the secondary winding of the transformer and a full-bridge rectifier implemented with the diodes D_{s1}~D_{s4}. The transformer's turn ratio is defined as: $n = N_s / N_p$, where N_s and N_p represent the numbers of turns of the primary and secondary windings, respectively.

In this paper, the two ports on the primary side of the transformer are connected to a PV panel and a battery. To make the two sources work simultaneously, the following requirement should be satisfied so that the battery can be charged from the PV panel via the switch S_2.

$$V_{1M} > V_{bat} \tag{1}$$

where V_{1M} is the maximum voltage of the PV panel; V_{bat} is the nominal voltage of the battery.

To simplify the analysis, the proposed converter is analyzed by two separate converters, where one is a single-switch LCL-resonant converter, and the other is the battery-related buck and boost converter consisting of L_2, S_2, and S_3.

B. Single-Switch LCL-Resonant Converter for PV Panel

In a switching period, the voltages across C_1 and C_s can be taken as constant values. Particularly, in the steady state, $V_{Cs} = V_1$, where V_1 is the converter input voltage. The converter has seven operating modes depending on the states of the switch S_1 and the resonant circuit. The differential equations of the resonant circuit in Mode k (k = 1, ···, 7) are

$$\begin{cases} v = L_r^{(k)} \cdot \dfrac{di_r^{(k)}}{dt} \\ i_1 = C_r \cdot \dfrac{dv}{dt} + i_r^{(k)} \end{cases} \tag{2}$$

where v represents the voltage of the capacitor C_r; $L_r^{(k)}$ and $i_r^{(k)}$ represents the equivalent resonant inductance and the current flowing through the equivalent resonant inductor in the k^{th} (k = 1, ···, 7) operating mode, respectively. Then v can be solved from (1) and is expressed in the following form.

$$v(t) = A_k \cos\left(\omega_k (t - t_k)\right) + B_k \sin\left(\omega_k (t - t_k)\right) + V_k^* \tag{3}$$

where ω_k is the resonant frequency in Mode k, V_k^* is the special solution of equation (2) in Mode k, and A_k and B_k are coefficients, which can be expressed as:

$$A_k = v(t_k) - V_k^* \tag{4}$$

$$B_k = \frac{I_1 - i_p(t_k) - i(t_k)}{\omega_k \cdot C_r} \tag{5}$$

where $v(t_k)$, I_1, $i_p(t_k)$, and $i(t_k)$ represent the voltage of C_r and the currents of L_1 (i_1 can be viewed as a constant value I_1 because of a large L_1), L_s, and L_r at time t_k, respectively. Equations (4) and (5) indicate that only ω_k and V_k^* are required to determine the parameters of (3).

The equivalent circuits and steady-state waveforms of the seven operating modes of the converter are shown in Figs. 2 and 3, respectively. To facilitate the explanation of the converter operation, define $V_T = V_{dc}/n$ the equivalent output voltage of the converter referred to the primary side of the transformer.

Mode 1: $t \in [t_1, t_2]$ (see Fig. 3). Prior to Mode 1, S_1 is off; the currents flowing through L_r and L_s are zero and a positive value of I_1, respectively, i.e., $i(t_1) = 0$, $i_p(t_1) = I_1$. When S_1 is on, as shown in Fig. 2(a), L_r and L_s resonate with C_r, the current of the inductor L_r increases and the voltage of the capacitor C_r decreases. Due to the existence of L_r, the current of the switch S_1 increases slowly so that the switch is turned on under the ZCS condition. The circuit equations in this mode can be expressed as:

$$\omega_1 = \frac{1}{\sqrt{\dfrac{L_r \cdot L_s}{L_r + L_s} \cdot C_r}} \tag{6}$$

$$V_1^* = \frac{L_r}{L_r + L_s} \cdot (V_1 + V_T) \tag{7}$$

In this mode, the current flowing through the primary magnetizing inductance L_m, i_m, increases. At the end of Mode

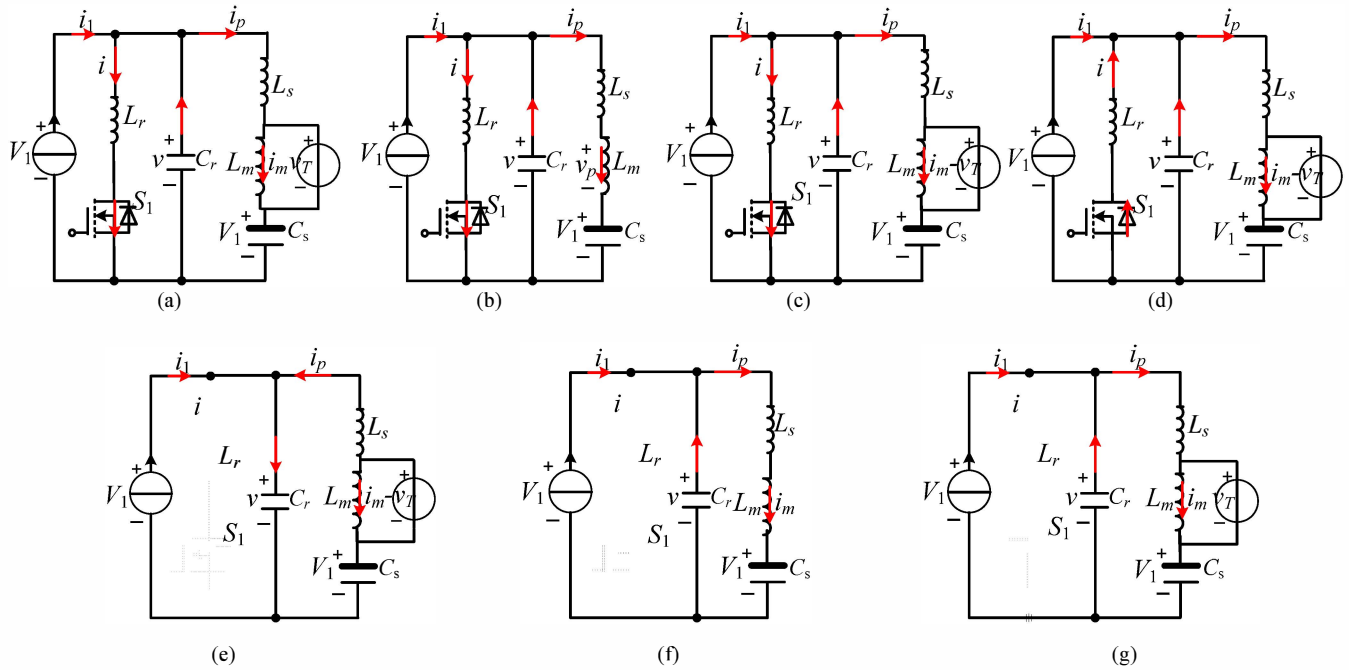

Fig. 2. Equivalent circuits for different operating modes. (a) Mode 1: S_1 is on, $i > 0$, $v_p = V_T$; (b) Mode 2: S_1 is on, $i > 0$ and $i_p = i_m$; (c) Mode 3: S_1 is on, $i > 0$, and $v_p = -V_T$; (d) Mode 4: S_1 is being turned off, $i < 0$ and $v_p = -V_T$; (e) Mode 5: S_1 is off, $i = 0$, $v_p = -V_T$; (f) Mode 6: S_1 is off, $i = 0$, $i_p = i_m$; (g) Mode 7: S_1 is off, $i = 0$, $v_p = V_T$.

1, $i_p(t_2) = i_m(t_2)$.

Mode 2: $t \in [t_2, t_3]$, during which S_1 is on, $i(t) > 0$, and $i_p(t) = i_m(t)$. As shown in Fig. 2(b), the primary magnetizing inductance L_m, leakage inductance L_s, and L_r resonate with

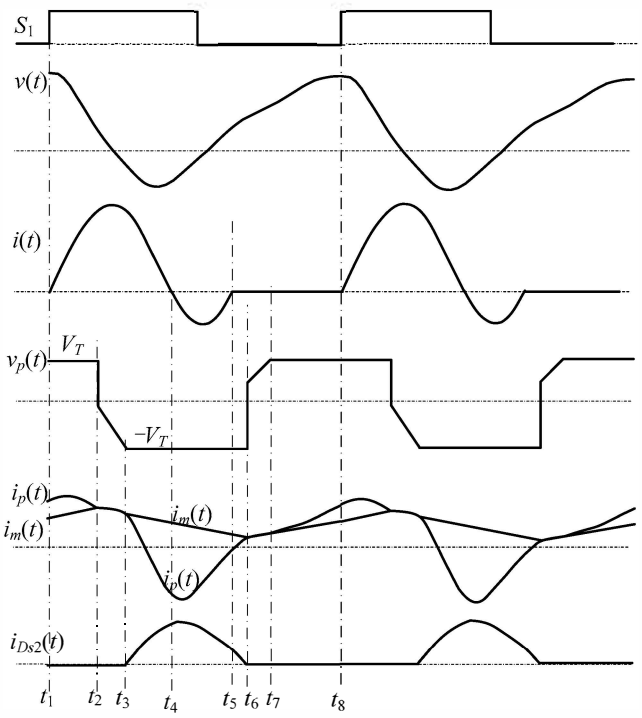

Fig. 3. Steady-state waveforms of the proposed converter.

C_r. Since $L_m >> L_s$, $L_m >> L_r$, then

$$\omega_2 \approx \frac{1}{\sqrt{\frac{L_r \cdot (L_s + L_m)}{L_r + L_s + L_m} \cdot C_r}} \approx \frac{1}{\sqrt{L_r \cdot C_r}} \tag{8}$$

$$V_2^* = \frac{L_r}{L_r + L_s + L_m} \cdot V \approx \frac{L_r}{L_m} \cdot V_1 \tag{9}$$

At the end of Mode 2, $v_p(t_3) = -V_T$, the diode D_{s2} begins to conduct.

Mode 3: $t \in [t_3, t_4]$, during which S_1 is on, $i(t) > 0$, $v_p(t) = -V_T$, $i_{Ds2} > 0$. As shown in Fig. 2(c), L_r and L_s resonate with C_r; the energy stored in L_r is released to charge the capacitor C_r; v_p is clamped to $-V_T$ and i_p changes its direction. The following equation can be obtained and $\omega_3 = \omega_1$,

$$V_3^* = \frac{L_r}{L_r + L_s} \cdot (V_1 - V_T) \tag{10}$$

This mode terminates at time t_4 when the current of L_r decrease to zero, i.e., $i(t_4) = 0$.

Mode 4: $t \in [t_4, t_5]$, during which S_1 is on, $i(t) < 0$, $v_p(t) = -V_T$, and $i_{Ds2} > 0$. As shown in Fig. 2(d), a negative current flows through the internal diode of the switch S_1; then the switch can be turned off at any time in this mode under the ZVS condition. The equation is the same as (10) in Mode 3. Thus, $\omega_4 = \omega_1$, $V_4^* = V_3^*$. At the end of Mode 4, $i(t_5) = 0$.

Mode 5: $t \in [t_5, t_6]$, during which S_1 is off, $i(t) = 0$, $v_p = -V_T$ and $i_{Ds2} > 0$. As shown in Fig. 2(e), L_r and the switch S_1 can be neglected in the circuit. The inductor L_s resonates with the capacitor C_r, and the direction of i_p changes from negative to

positive. The equations are expressed as:

$$\omega_5 = \frac{1}{\sqrt{L_s \cdot C_r}} \tag{11}$$

$$V_7^* = V_1 - V_T \tag{12}$$

At the end of Mode 5, $i_p(t_6) = i_m(t_6)$, $i_{Ds2}(t_6) = 0$, and v_p changes its polarity from negative to positive at t_6.

Mode 6: $t \in [t_6, t_7]$, during which S_1 is off, $i(t) = 0$, $i_p(t) = i_m(t)$, L_m and L_s resonate with C_r, and C_r is charged in this mode.

$$\omega_6 = \frac{1}{\sqrt{(L_s + L_m) \cdot C_r}} \tag{13}$$

$$V_6^* = V_1 \tag{14}$$

At time t_7, $v_p(t_7) = V_T$.

Mode 7: $t \in [t_7, t_8]$, during which S_1 is off, $i(t) = 0$, $v_p(t) = V_T$, L_s resonates with C_r, then $\omega_7 = \omega_5$, and

$$V_7^* = V_1 + V_T \tag{15}$$

Once S_1 is turned on, Mode 7 switches to Mode 1.

C. *Buck and Boost Converter for Battery*

The buck and boost converter consists of the inductor L_2, switches S_2 and S_3, and capacitor C_s. When the generated solar power is larger than the power required by the load, S_3 is inactive and S_2 is switched on to form the buck converter. Then, the surplus energy generated from the PV panel is stored in the battery. In contrast, when the generated solar power is less than the power required by the load, S_2 is switched off and S_3 is switched on to form the boost converter. The battery is discharged to C_s to provide the deficient energy required by the load.

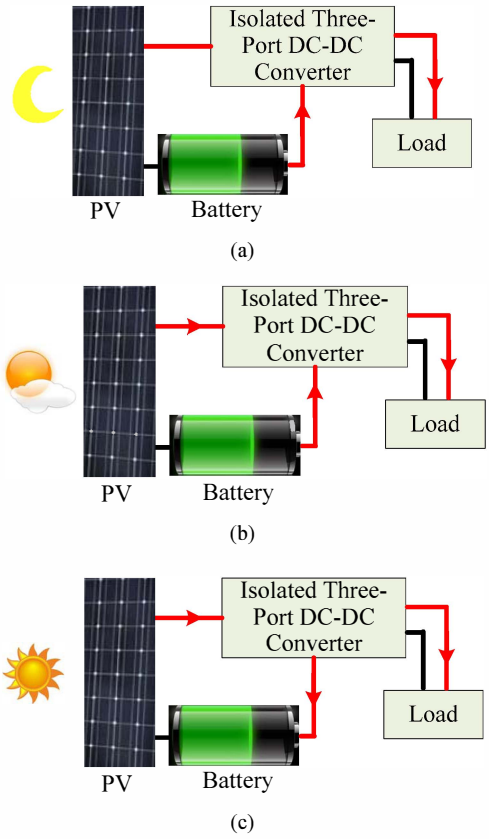

Fig. 4. Three working modes of the converter (The arrows show the directions of energy flow). (a) Mode 1: There is no solar energy available and battery is discharged to supply load; (b) Mode 2: PV works in MPPT mode and battery works in discharge mode to provide the deficient energy; (c) Mode 3: PV works in MPPT mode and the battery works in charge mode to absorb the surplus solar energy.

III. Power Management of the Proposed Controller

Two controllers are needed to manage the power in the LVS. Their objectives are to regulate the output DC-link voltage to a constant value and manage the power for the two sources, respectively. According to the availability of the solar power, there are three working modes of the converter.

A. *Three Working Modes*

Fig. 4 shows the three working modes of the converter. As shown in Fig. 4(a), in Mode 1, there is no solar power. Thus, the battery is discharged to supply the load. The active switches are S_1 and S_3. The purpose of the boost converter (by controlling S_3) is to regulate the voltage of C_s to a constant value; while the PV converter (by controlling S_1) is to maintain the output voltage to a constant value using a frequency modulation method.

In Mode 2, there is solar radiation but the solar power is not sufficient to supply the load. The PV panel is operated in the MPPT mode to generate the maximum power. On the other hand, the deficient power is supplied by the battery so that the output voltage can be maintained at a constant value. In this mode, the PV converter is controlled by the MPPT algorithm described later, and the battery is discharged by the boost converter.

In Mode 3, the available solar power is more than the load demand. As in Mode 2, the PV converter works in the MPPT mode and the battery is charged by controlling the duty ratio of S_2.

Proper controllers are designed to manage the power in different modes. Fig. 5 shows the overall system with controllers, which include a MPPT controller for the PV panel and charge and discharge controllers for the battery.

B. *MPPT Controller for PV Panel*

The proposed converter is applied for MPPT control of a PV panel. The algorithm implemented in the controller is the perturbation and observation (P&O) MPPT algorithm [12] to maximize the PV panel's output efficiency. Fig. 6 shows the flowchart of the algorithm. A ratio r_c is defined to specify the relative power change (RPC) of the PV panel between two consecutive sampling steps.

$$r_c = \frac{|P_1(k) - P_1(k-1)|}{P_1(k-1)} \tag{16}$$

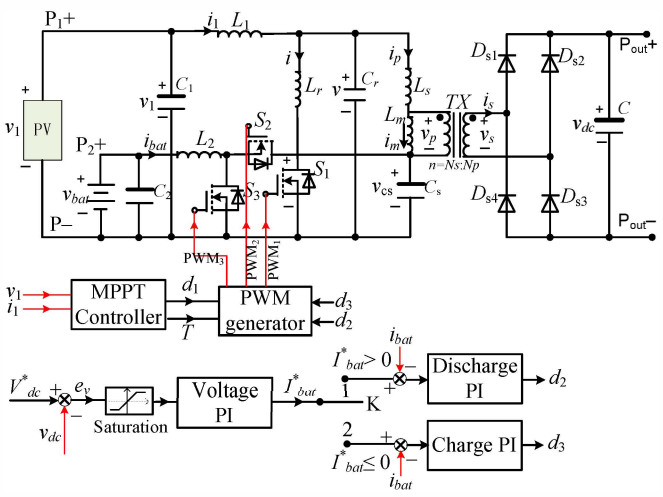

Fig. 5. Overall block diagram of the system with controllers.

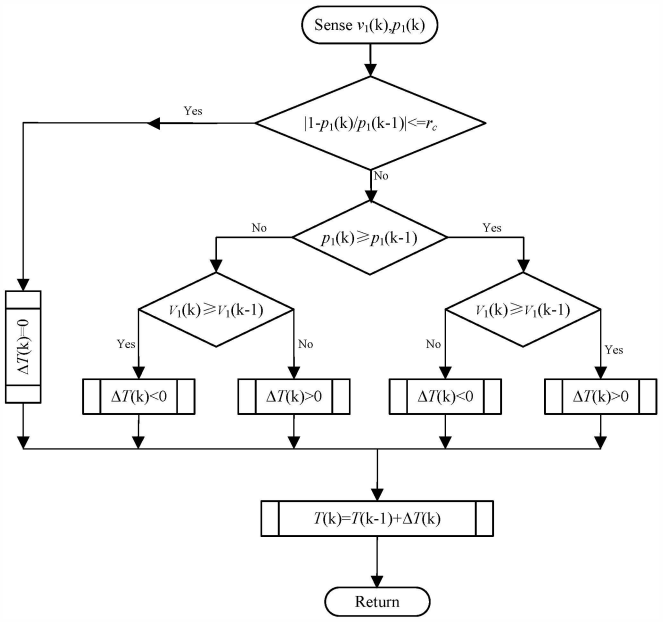

Fig. 6. The flowchart of the MPPT algorithm.

where $P_1(k)$ and $P_1(k-1)$ represent the measured output power of the PV panel in the k^{th} and $(k-1)^{th}$ steps, respectively.

It can be seen that for the same power variation value, r_c is proportional to $1/P_1(k-1)$. In this paper, the switching period (T) will not be changed if the RPC is lower than a predefined value (e.g., 10^{-4}). The on time of S_1 is fixed as 4.2 μs so that S_1 can achieve soft switching.

C. Controllers for Battery

Figs. 7(a) and (b) show the equivalent circuit of the battery and the converter when the battery works in the charge and discharge mode, respectively. To simplify the analysis, a resistor and a capacitor are used to model the battery in the charge mode, as shown in Fig. 7(a), and the converter is a buck converter. Then the transfer function of the battery current (i_{bat}) with respect to the duty ratio of the switch S_2 (d_2) can be derived:

$$G_c(s)=\frac{i_{bat}(s)}{d_2(s)}=\frac{\frac{V_{bat}}{L_2}\left(s+\frac{1}{R_c\cdot C_2}\right)}{s^2+\left(\frac{r}{L_2}+\frac{1}{R_c\cdot C_2}\right)s+\frac{1}{L_2\cdot C_2}} \quad (17)$$

where R_c represents the equivalent load of the battery, C_2 is the capacitance of the battery, and r is the parasitic resistance of the inductor L_2.

Similarly, in the discharge mode, the transfer function of i_{bat} with respect to the duty ratio of switch S_3 (d_3) is:

$$G_d(s)=\frac{i_{bat}(s)}{d_3(s)}=\frac{\frac{V_{cs}}{L_2}\left(s+\frac{1}{R_d\cdot C_s}\right)+\frac{I\cdot(1-D_3)}{L_2\cdot C_s}}{s^2+\left(\frac{r}{L_2}+\frac{1}{R_d\cdot C_s}\right)s+\frac{(1-D_3)^2}{L_2\cdot C_s}} \quad (18)$$

where R_d is the equivalent load of the battery in the discharge mode; D_3 is the steady-state value of d_3.

To control the current of the battery, a proportional-integral (PI) controller ($K_p + K_i/s$) is used, as shown in Fig. 5. The battery current controller takes the current error as the input and generates the duty ratio of S_2 (S_3) in the charge (discharge) mode. When the reference current I^*_{bat} is negative, the charge controller is selected such that $d_2 > 0$ and $d_3 = 0$. Otherwise, when the reference current I^*_{bat} is positive, the discharge controller is selected such that $d_3 > 0$ and $d_2 = 0$. Once the current controller is designed, the voltage controller which has a lower cutoff frequency than the current loop is then designed. The PI parameters of the current and voltage controllers used in this paper are listed in Table I.

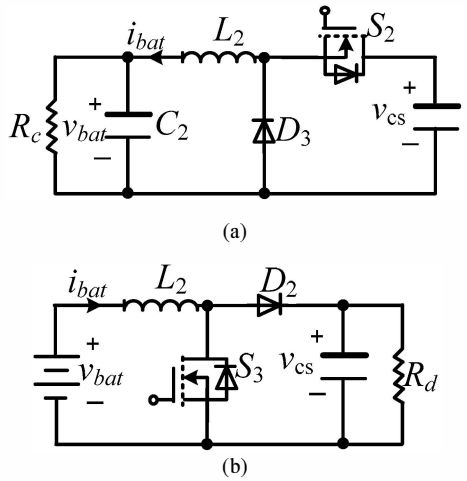

Fig. 7. Equivalent circuit of the battery with (a) the buck converter in charge mode and (b) the boost converter in discharge mode.

Table I: Parameters of the current and voltage controllers.

	K_p	K_i
Current controller (charge)	0.2	50
Current controller (discharge)	0.192	30
Voltage controller	10	2

IV. Simulation Results

Simulations are carried in MATLAB/Simulink to validate the proposed converter and the controllers. The parameters of the converter are as follows: transformer turn ratio n = 4, resonant inductance L_r = 3.2μH, resonant capacitance C_r = 0.44μH. A SunWize SW-S110P PV panel is used, whose open-circuit voltage (V_{oc}) and the short-circuit current (I_{sc}) are 22 V and 6.6 A, respectively. The battery consists of three Samsung ICR18650-28A rechargeable lithium-ion cells connected in series. The nominal voltage, standard charging current, and the capacity of each battery cell are 3.75V, 1.4A, and 2800mAh, respectively. Thus, the nominal voltage of the three-cell battery is 11.25 V. The allowed switching frequency varies from 90 kHz to 125 kHz. The desired DC-link voltage (V^*_{dc}) and power of the load are 50 V and 50 W, respectively.

To test the dynamic characteristic of the controllers, the solar radiation is step changed to examine the responses of the DC-link voltage and output power of the PV panel, as shown in Fig. 8. Fig. 8(a) shows that the initial solar radiation is zero and there is no power generated by the PV panel, as shown in Fig. 8(c). This indicates that the converter works in Mode 1 and all of the power is supplied by discharging the battery. Fig. 8(b) shows that the DC-link voltage quickly reaches its reference value of 50 V.

Mode 1 does not terminate until the solar radiation changes from zero to 400 W/m^2 at the 1st second. After that, the maximum power generated by the PV panel is 40 W, which is less than the load demand of 50 W. Thus, the battery still works in the discharge mode to provide the deficient power required by the load and the variation of the DC-link voltage is small.

Between 1 second and 1.5 second, the converter works in Mode 2. The PV panel generates the maximum power as indicated in Fig. 8(c).

At 1.5 second, the solar radiation is changed from 400 W/m^2 to 600 W/m^2, which corresponds to 60-W maximum power. Then the battery stops discharging and starts to absorb the surplus power generated from the PV panel. It takes some time to change the direction of the battery current, which not only results in approximately 2-V overshoot in the DC-link voltage during the transient period, but also leads to the PV power generated less than the ideal maximum power, as shown in Fig. 8(c). After 0.3 seconds, both the output voltage and PV power reach the desired value and the ideal maximum power point (MPP), respectively.

It should be noted that in the real application, the slew rate of the solar radiation is not so large. To testify the

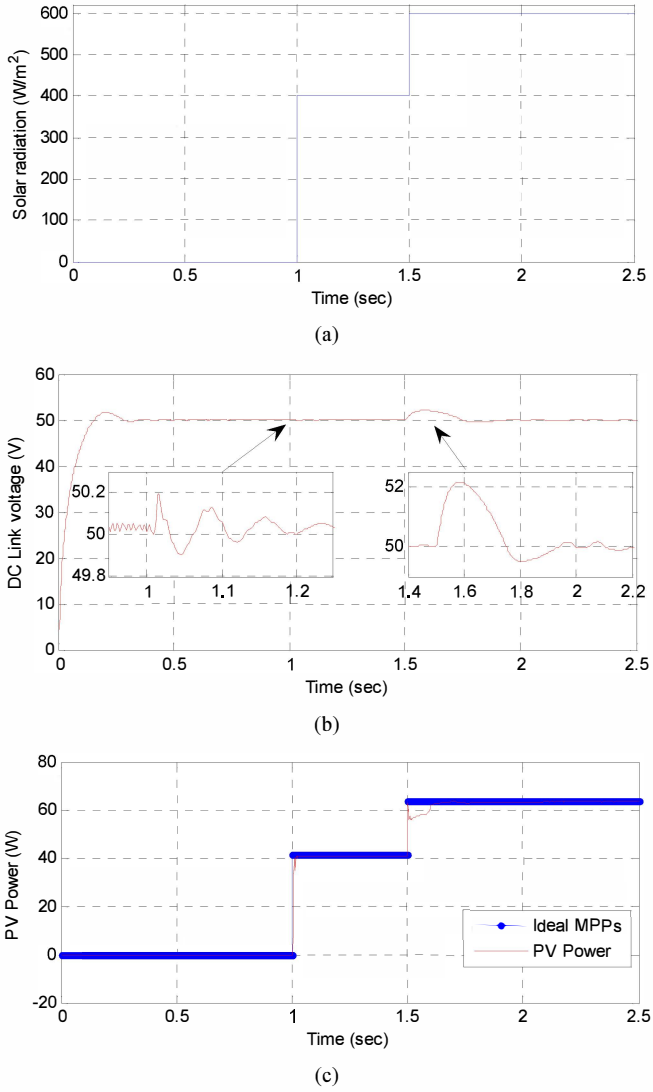

Fig. 8. Step responses. (a) The profile of solar radiation; (b) DC-link voltage response; (c) PV power response.

effectiveness of the converter and its control algorithm, the data provided by the National Renewable Energy Laboratory (NREL) [13] was used. The data was collected from the South Table Mountain site in Golden, Colorado, on Feb. 7, 2013. In the simulation, the time period is compressed from original 11 hours to 16 seconds, which means that the rate of change of the solar radiation data in the simulation is around 2400 times larger than the actual value. Fig. 9 shows the simulation results of the PV power and the DC-link voltage. As shown in Fig. 9(a), the energy extracted from the PV panel closely follows the ideal MPP by using the proposed converter and MPPT control algorithm. The output voltage achieves its desired value of 50 V within 0.3 second and the error is less than 1.2%. The steady-state voltage error is less than 0.6%.

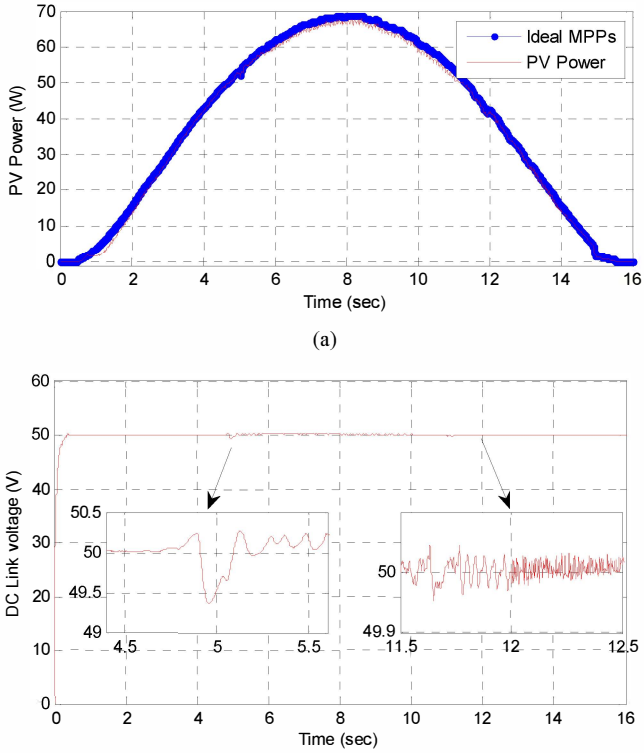

Fig. 9. Simulation results with NREL data. (a) The generated PV power; (b) the DC-link voltage.

V. Experiment Results

The system simulated is constructed in hardware to further validate the proposed converter and control algorithm via experimental studies. Fig. 10 shows the prototype of the whole system. It consists of the proposed DC-DC converter, which is connected to a SunWize SW-S110P PV panel, a battery, a resistive load, and an eZdsp F2818 control board. The control algorithm is implemented in a TMS320F2812 DSP located on the control board.

The parameters of the system are the same as those used in the simulation except for the desired DC-link voltage, which is 30 V in the experimental system. Fig. 11 shows the steady-state waveforms when the converter works in Mode 1. i.e., there is no solar radiation and the battery is discharged to supply the load. As shown in Fig. 11(a), the positive battery current (i_{bat}) indicates that the battery works in the discharge mode. The DC-link voltage (v_{dc}) is close to the reference value of 30 V, which demonstrates the effectiveness of the discharge controller. Fig. 11(b) shows the waveforms of the main switch S_1. The voltage across the main switch drops to zero before the current increases, which indicates that the main switch has achieved ZVS when turning on. When the

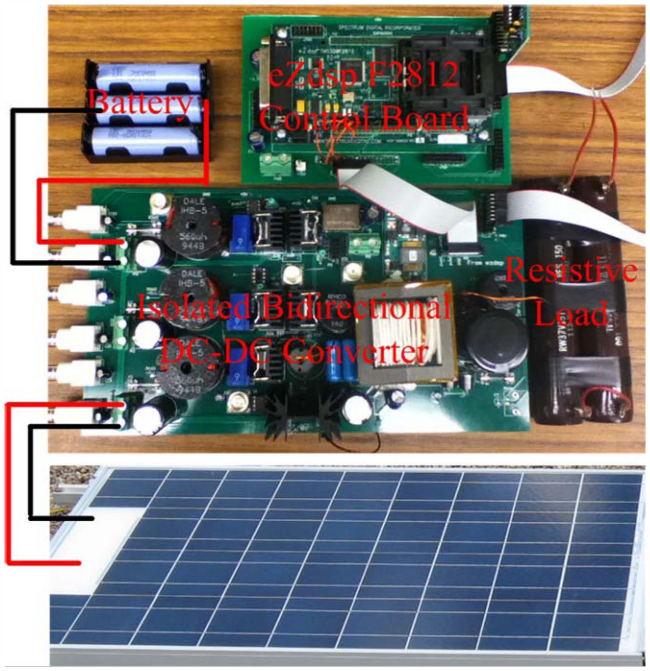

Fig. 10. The experimental system setup.

main switch is turned off, its current is not exactly zero. However, current (0.5A) flowing through the main switch when it is turned off is much less than its average current (2.86A). This indicates that the main switch has approximately achieved ZCS when turning off.

Fig. 12 shows the steady-state waveforms when the converter works in Mode 2. Compared to Mode 1, the battery current decreases from 3.3 A to 1.3 A in Mode 2, which indicates that in Mode 2 the battery provides less energy than it does in Mode 1. The deficient energy is provided by the PV panel, which can be seen from its positive current (i_1). Moreover, the DC-link voltage is also well controlled at the desired value.

VI. Conclusions

This paper has proposed a new isolated, three-port, bidirectional, DC-DC converter which uses the minimum number of switches. The proposed converter has been used for simultaneous power management of multiple energy sources, i.e., a PV panel and a battery, in this paper. Simulation results have shown that the converter is not only capable of MPPT for the PV panel when there is solar radiation, but also can control the charge/discharge of the battery to maintain the DC-link voltage at a constant value. The proposed converter is applicable to other types of renewable energy sources, e.g., wind turbine generators.

978-1-4673-5202-4/12/$31.00 © 2013 IEEE

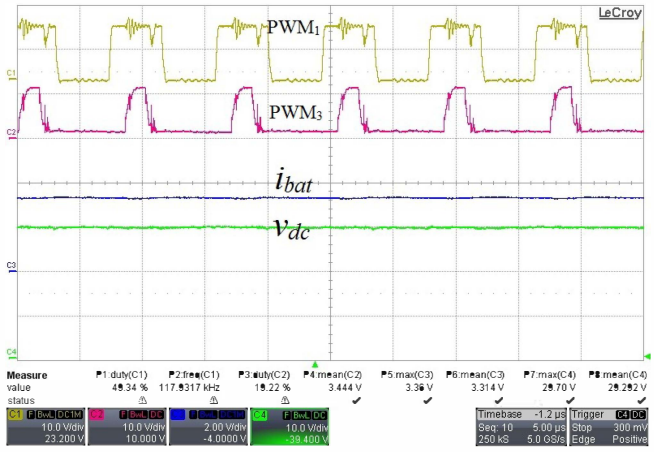

(a)

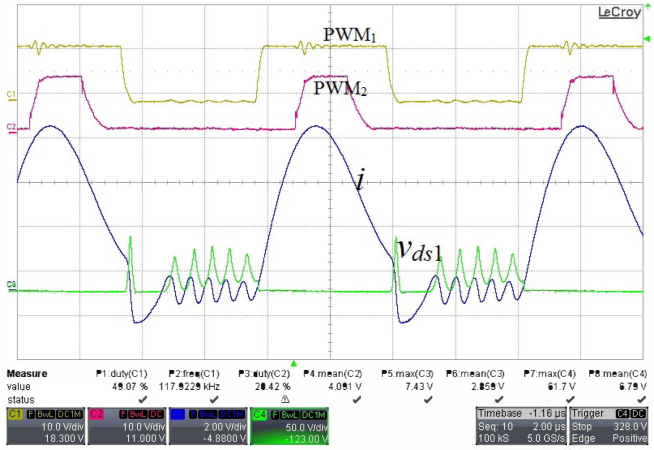

(b)

Fig. 11. The steady-state waveforms when the converter works in Mode 1. (a) Battery current and the DC-link voltage (CH2: 1A/V); (b) the current and voltage waveforms of the main switch S_1 (CH3: 1A/V).

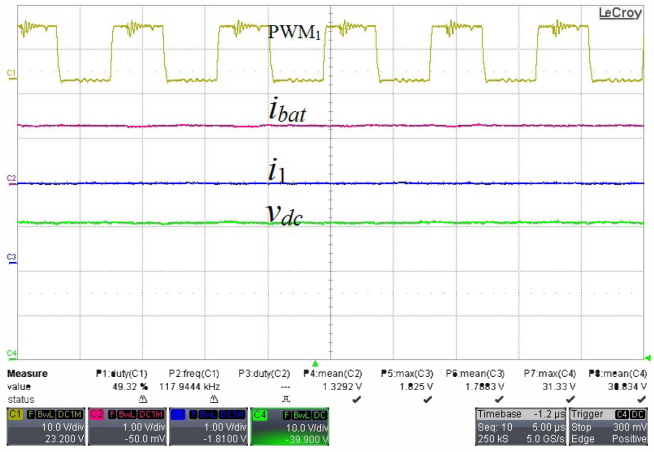

Fig. 12. The steady-state waveforms when converter works in Mode 2. (CH2: 1A/V, CH3: 1A/V)

REFERENCES

[1] C. Onwuchekwa and A. Kwasinski, "A modified-time-sharing switching technique for multiple-input DC-DC converters," *IEEE Trans. Power Electronics*, vol. 27, no. 11, pp. 4492-4502, Nov. 2012.

[2] Z. Qian, O. Abdel-Rahman, and I. Batarseh, "An Integrated four-port DC/DC converter for renewable energy application," *IEEE Trans. Power Electronics*, vol. 25, no. 7, pp. 1877-1887, Jul. 2010.

[3] Y. Chen, Y. Liu, and F. Wu, "Multi-input DC/DC converter based on the multi winding transformer for renewable energy applications," *IEEE Trans. Industrial Application*, vol. 38, no. 4, pp. 1096-1104, Aug. 2002.

[4] Y. Lembeye, V. Bang, G. Lefevre, and J. Ferrieux, "Novel half-bridge inductive DC–DC isolated converters for fuel cell applications," *IEEE Trans. Energy Conversion*, vol. 24, no. 1, pp. 203-210, Mar. 2009.

[5] J. Zeng, W. Qiao, and L. Qu, "An isolated multiport dc-dc converter for simultaneous power management of multiple renewable energy sources," in *Proc. IEEE Energy Conversion Congress and Exposition*, Sept. 2012, pp. 3741-3748.

[6] H. Tao, A. Kotsopoulos, J. Duarte, and M. Hendrix, "Family of multiport bidirectional DC-DC converters," *IEE Proc. Electric Power Applications*, vol. 153, no. 3, pp. 451- 458, May 2006.

[7] C. Zhao, S. Round, and J. Kolar, "An isolated three-port bidirectional dc-dc converter with decoupled power flow management," *IEEE Trans. Power Electronics*, vol. 23, no 5, pp. 2443-2453, Sept. 2008.

[8] J. Duarte, M. Hendrix, and M. Simoes, "Three-port bidirectional converter for hybrid fuel cell systems," *IEEE Trans. Power Electronics*, vol. 22, no. 2, pp. 480-487, Mar. 2007.

[9] G. Su and F. Peng, "A low cost, triple-voltage bus DC-DC converter for automotive applications," in *Proc. IEEE Applied Power Electronics Conference and Exposition,* Mar. 2005, pp. 1015-1021.

[10] D. Liu and H. Li, "A ZVS bi-directional DC-DC converter for multiple energy storage elements," *IEEE Trans. Power Electronics*, vol. 21, no. 5, pp. 1513-1517, Sept. 2006.

[11] H. Al-Atrash, F. Tian, and I. Batarseh, "Tri-modal half-bridge converter topology for three-port interface," *IEEE Trans. Power Electronics*, vol. 22, no. 1, pp. 341-345, Jan. 2007.

[12] C. Hua, J. Lin, and C. Shen, "Implementation of a DSP-controlled photovoltaic system with peak power tracking," *IEEE Trans. Industrial Electronics*, vol. 45, no. 1, pp. 99-107, Feb. 1998.

[13] http://www.nrel.gov/midc/apps/go2url.pl?site=BMS&page=day.pl?BMS.